Marine and Petroleum Geology 122 (2020) 104652

Contents lists available at ScienceDirect

Marine and Petroleum Geology

journal homepage: www.elsevier.com/locate/marpetgeo

Research paper

Geocellular rendering of cave surveys in paleokarst reservoir models

Bjarte Lønøy [a,b,*], Jan Tveranger [a], Christos Pennos [b], Fiona Whitaker [c], Stein-Erik Lauritzen [b]

[a] NORCE – Norwegian Research Centre AS, Nygårdsgaten 112, 5008, Bergen, Norway
[b] University of Bergen, Department of Earth Science, Allégaten 41, 5020, Bergen, Norway
[c] University of Bristol, School of Earth Sciences, Queens Rd, Bristol BS8 1QE, United Kingdom

ARTICLE INFO

Keywords:
Paleokarst
Reservoir modelling
Cave survey data
Geocellular rendering
Karst morphology

ABSTRACT

Infilled and collapsed cave systems are an important component of many paleokarst reservoirs. Incorporating these features into industrial reservoir models commonly relies on geostatistical modelling methods that often fail to capture key aspects of connectivity, geometry and volume of the paleokarst features realistically. The present work investigates the implementation of realistic cave geometries in geocellular models using survey data from an active karst cave as a starting point. The proposed method utilizes cave survey data to generate a dense equally spaced point-cloud representing the cave system. The point-clouds are used for geometric modelling and subsequent geocellular discretization of the karst system. The volumetric and geometric accuracy of this novel reservoir modelling method is compared to that from two established methods by benchmarking against the cave survey data. Additionally, the interlinkage between grid cell resolution, applied filter cut-off and geocellular rendering are evaluated. This study demonstrates that our proposed novel methodology can provide an excellent geometric and volumetric geocellular rendering of karst systems using cave survey data as input. Employing a combination of cave network maps and forward modelling of collapse and infill may enable model rendering of these features that more closely echoes processes controlling cave and karst breccia formation and geometric characteristics. In turn, this could offer better constraints to forecast paleokarst reservoirs architecture and properties.

1. Introduction

Active epigene and hypogene karst systems are the precursors of paleokarst reservoirs and can be used as analogues for geometric configurations of paleokarst formed under given stratigraphic, tectonic and environmental constraints. The geometry and setting of existing caves can also form the starting point for forward modelling of collapse and infill processes. Thus, cave surveys form an important, and for reservoir modelling largely unused, source of data for generating paleokarst reservoir analogue models. A first step to facilitate the general use of this data to study subsurface flow behaviour in these systems is to provide workflows for rendering cave survey data in reservoir models using standard industrial software.

Karst systems, consisting of open and partially- or completely infilled conduits and cavities, can provide key insights into the numerous paleokarst reservoirs worldwide. Well-studied examples include the Yates field of West Texas (Craig, 1988; White et al., 1995), the Golden Lane fields in Mexico (Coogan et al., 1972; Blickwede and Rosenfeld, 2010), the Rospo Mare field in Adriatic Sea (Soudet et al., 1994), the Casablanca field in the offshore Spain (Lomando et al., 1993), the Kharyaga field in the Russian Arctic (Zempolich and Cook, 2002), the Kashagan field in Kazakhstan (Kaiser and Pulsipher, 2007), the Kirkuk field in Iraq (Trice, 2005), and the Tahe field of the Tarim Basin in China (Yan, 2002). Although boasting some of the most productive wells in oil history (Viniegra and Castillo-Tejero, 1970; Fournillon et al., 2012), the recovery factor (RF) from karst-related reservoirs is generally very low when compared to conventional carbonate- and organic build-up reservoirs (Sun and Sloan, 2003; Montaron, 2008; Montaron et al., 2014). Also, production from these reservoirs is often associated with issues such as rapid water breakthrough, bypass flow and drill-bit drops.

Some of the biggest challenges for improving paleokarst reserve estimations relate to volumetric determination and estimation of cave geometries and cave size statistical distributions, which directly impact on hydrocarbon recovery factors (Montaron et al., 2014). The spatial distribution and associated morphology of karst networks play a significant role in subsurface fluid flow behaviour (e.g. Chaojun et al., 2010; Tian et al., 2016), and has been recognized in many carbonate reservoirs (Rongier et al., 2014). Hence, robust reservoir models

* Corresponding author. NORCE – Norwegian Research Centre AS, Nygårdsgaten 112, 5008, Bergen, Norway.
E-mail address: bjarte.lonoy@norceresearch.no (B. Lønøy).

https://doi.org/10.1016/j.marpetgeo.2020.104652
Received 30 May 2020; Received in revised form 5 August 2020; Accepted 8 August 2020
Available online 15 August 2020

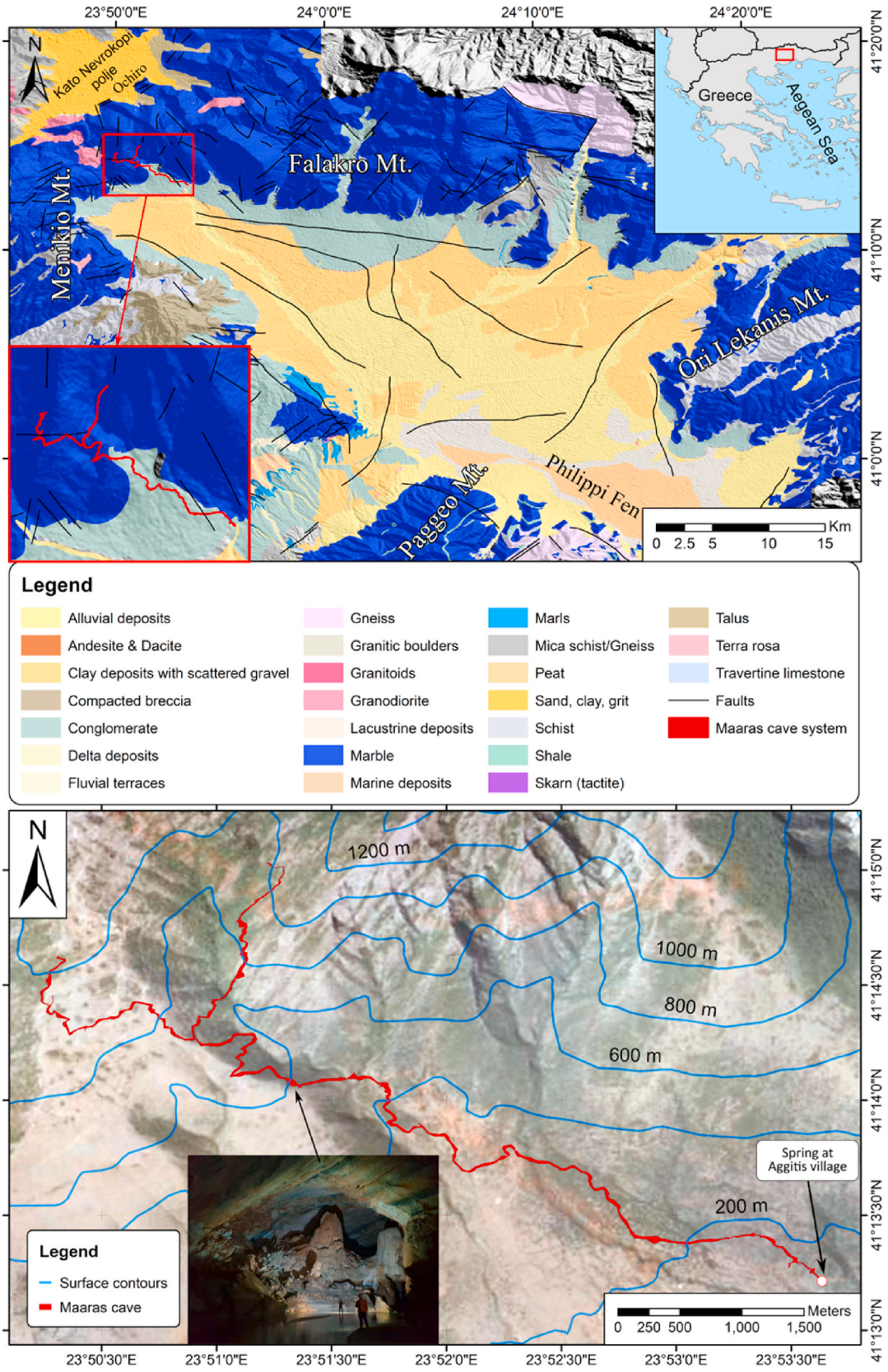

Fig. 1. An overview map of the modelled cave and surrounding area. Upper: Maaras cave (red) superimposed on a geological map modified from Pennos et al. (2016b) and a digital elevation model (ASTER GDEM). Insert: Close up of Maaras cave system. Lower: Outline of Maaras cave (from cave survey) with contour lines. Insert: picture to highlight cavern dimensions and interior. Note persons for scale. Orthophotographic map: www.ktimatologio.gr(For interpretation of the references to colour in this figure legend, the reader is referred to the Web version of this article.)

capturing the spatial distribution, morphology, and volume of paleokarst features are essential to improve resource estimates and facilitate low-risk well- and production planning.

Most current paleokarst reservoir models are based on stochastic simulations using various statistical methods such as "Object Based Modelling" (OBM), "Multiple Point Statistics" (MPS) or fast marching approach, which are conditioned on available well-data (e.g. Borghi et al., 2010; Erzeybek Balan, 2012; Rongier et al., 2014). However, this approach largely fails to adequately incorporate the geometry, volume and connectivity characteristics of karst features. Considering these difficulties, using a more concept-driven approach (rather than a data-driven) employing extant information about realistic karst cave systems as a starting point, seems to offer potential. As pointed out by Trice (2005), the use of use conceptual karst models is essential to understand the effect on karstification, and by extension, karst-degradation, infill and diagenesis of former karst systems on reservoir quality. In this context, recent cave systems are a natural starting point for generating analogues for geometries and infill features. Standard reservoir modelling software suites used by the petroleum industry currently have no established workflows or dedicated add-ins for handling the geometries and property distributions that characterize paleokarst reservoirs. Developing methods and workflows to handle this is a prerequisite for further work. Labourdette et al. (2007) address some of these issues from a non-epigenic viewpoint, and their results show that speleogenesis of flank-margin caves can be modelled with a close resemblance and coherence to field data using a combination of deterministic and stochastic methods. However, karst development on carbonate islands are typically controlled by the freshwater lens configuration (Mylroie and Carew, 1995), resulting in cave patterns different to those commonly associated with epigene karst systems (Palmer, 1991). Here, the primary focus is presenting a new methodology ("proof of concept") for geocullar rendering of epigenic karst system, but the proposed method may also be suitable for hypogenic- and flank margin karst systems.

The pioneering work of Furnée (2015) and Ledsaak (2016) produced two different approaches for incorporating geometrically complex karst systems into reservoir models by employing available tools. Their studies highlighted that although feasible to implement, geometries were either rendered oversimplified when transferred to geocellular grids, or required substantial and time-consuming editing to match observations (Lønøy et al., 2019b).

Building on these previous efforts, the present study outlines a quick and robust workflow for importing cave survey data into geocellular reservoir models in order to use these as starting points for forward modelling of collapse and infill, forward seismic modelling and fluid flow simulation. The study aims to evaluate the volumetric and geometric accuracy of the modelling methods as well as appraise the interlinkage between grid cell resolution, applied filter cut-off and geocellular rendering. The models in this study are based on a survey of the Maaras cave system, an active cave system in northern Greece (Pennos et al., 2016b).

2. Cave system analogue

2.1. Maaras cave

The Maaras cave is an almost 12 km long cave system which has developed parallel to the north-western margin of the Aggitis river basin in the prefecture of Eastern Macedonia in northern Greece (Fig. 1). The cave is developed within the marbles of the Rhodope massif, and four speleogenetic phases associated with changes in local base-level have been identified (Pennos et al. (2016b); and references within). Maaras cave hosts an active river system which exits the subsurface as a spring at 123 m.a.m.s.l. near the village of Aggitis. The mapped length of the cave is 10441 m, with the innermost mapped position located 71 m above the current level of the spring (Pennos et al., 2016a). The river slope varies

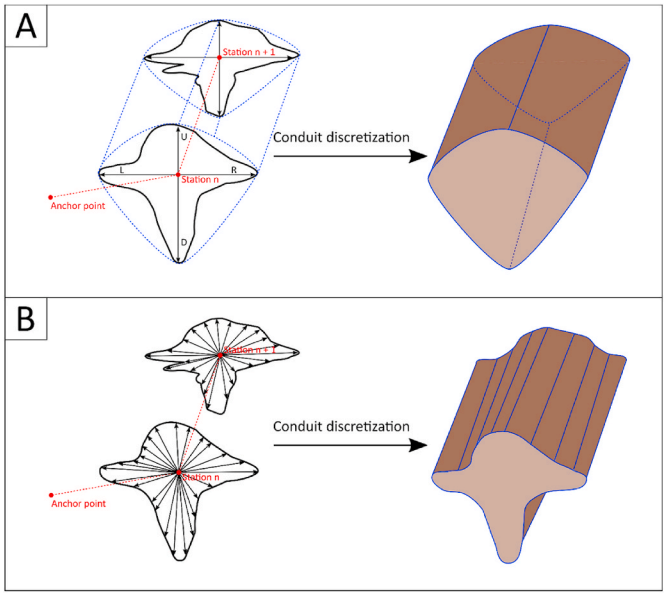

Fig. 2. Conceptual models of cave surveying techniques and conduit discretization. A) A simple cave survey method consisting of five measurements for each survey station: floor, roof, left, right wall and new survey station. B) Modern cave survey method consisting of multiple measurements from each survey station. Note that opposing measurements are not necessarily parallel and thus LRUD data derived from this method represent the maximum distance or a manually selected point for each direction. A higher density of shots increases the cross-sectional geometric resolution.

throughout the cave, from 3% to 67%, with steepest slopes occurring near the spring (Pennos et al., 2016b). The cave shows two shorter tributary passages; a western branch and an eastern branch that join to form a more extended master conduit to the spring (see Fig. 1). The cave system has no closed loops, but exhibits a pattern of lower-order passages joining tributaries to form higher-order passages; a cave morphology resembling the typical branchwork type as classified by Palmer (1991).

The cave is partly filled by thick accumulations of sandy clastic sediments, creating a relatively flat cave floor. Electric resistivity tomography (ERT) in some parts of the cave reveals that locally the sedimentary thickness exceeds 45m (Fikos et al., 2019; Lønøy et al., 2019a), filling 80–95% of the total karst cavity height. In contrast to the flat sediment floor, the cave roof has irregular morphology and cavity height varies from a few cm up to 60m; following a looping pattern.

3. Methodology

Methods and workflows for implementing traditional cave survey data into industry-standard reservoir modelling tools have previously been described by Furnée (2015) and Ledsaak (2016). The two workflows, hereafter labelled Method 1 and Method 2 respectively, are summarized below, and are used for comparison with the new method outlined in the present study (Method 3). The new workflow (Method 3), employs a combination of open source and commercial software used by the industry: PocketTopo (Heeb, 2010), Therion (Budaj and Stacho, 2019), MATLAB™ (MATLAB, 2010) and RMS™ (Roxar, 2018). The same results may be achieved using different software with similar functionalities. Terminology and functions mentioned in this article will refer to those presented and offered by the applied software.

If not stated otherwise, all grid models have a global grid resolution of 2 × 2 × 2m (X,Y,Z) and all mapped surfaces comprise a 2 × 2m (X,Y) grid resolution.

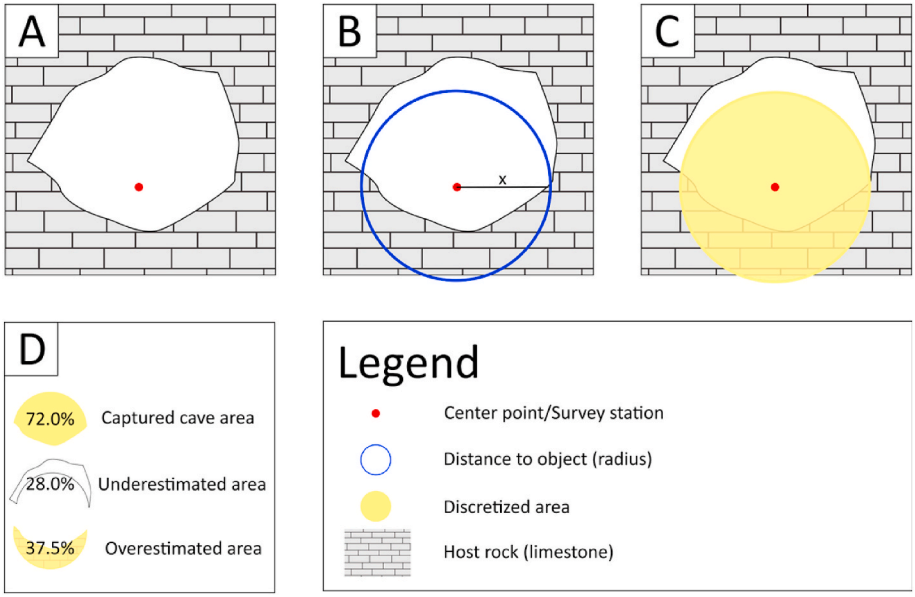

Fig. 3. Cross-sectional illustration of the workflow suggested by Furnée (2015) (Method 1). A) The centre points (red dot) is used as input for geometric modelling B) A cut-off value based on the "distance to object" calculation (blue circle) is set to delineate the estimated cave C) Final discretized cave area (yellow circle). D) Area coverage; area calculations based on image analysis from the illustration, show that for this example, 72.0% of the original cave area is discretized by this method. However, based on the illustration, the method fails to discretize 28.0% of the original cave area and overestimate the total area by 9.5%. Note that a smooth circular discretized area is used to illustrate the concept and that a geocellular representation would have a more "jagged" discretization, reflecting the grid cells. Also note that the over- or underestimation of the conduits cross-sectional area will largely depend on the spatial arrangement of the survey station (red dot) and applied filter (see Section 5). (For interpretation of the references to colour in this figure legend, the reader is referred to the Web version of this article.)

3.1. Cave surveying

Over the past decade, advanced terrestrial LiDAR instruments and photogrammetry have been introduced for cave mapping (e.g. Lerma et al. (2010); Gede et al. (2013); Gallay et al. (2015); Gallay et al. (2016), allowing high-resolution three-dimensional cave mapping. However, most modern cave surveys are still carried out using simple digital equipment such as laser rangefinders (e.g. Leica™ Disto X310) in combination with a handheld computer (e.g. a personal digital assistant - PDA) (http://paperless.bheeb.ch/). Conventional cave surveys consist of a series of consecutive line-of-sight measurements between survey-stations anchored to a geo-referenced point (often at the cave entrance). The stations can either be temporary or permanently marked locations and are chosen based on ease of access and line-of-sight to neighbouring stations. The rangefinder records distance, direction (azimuth) and inclination from horizontal (dip) between stations. The handheld computer display data numerically and graphically and can be used to store and manage measured data; allowing the addition of sketches directly on the screen. Moreover, the measurements between stations and the distance to the corridor walls (left, right, up, down – LRUD (Fig. 2A) or more points (Fig. 2B)) at a given station can be recorded to create a relatively high-resolution geometric representation of the cross-sectional shape of the conduits (Heeb, 2008, 2009, 2014).

The Maaras cave survey (Pennos et al., 2016b), applied here, was carried out using modern surveying techniques and includes multiple wall measurements for each survey station (e.g. Fig. 2B).

3.2. Method 1

The workflow for Method 1 (Furnée, 2015) comprises three steps (Fig. 3). The method assumes that the survey stations are centre points within the cave passage and generates a polygon ("skeleton line") by connecting the points. The skeleton line is then refined to generate additional, more densely spaced points along the line segments (between the survey stations). These points are used as input for geometric modelling. The geometric modelling function in RMS™, allows

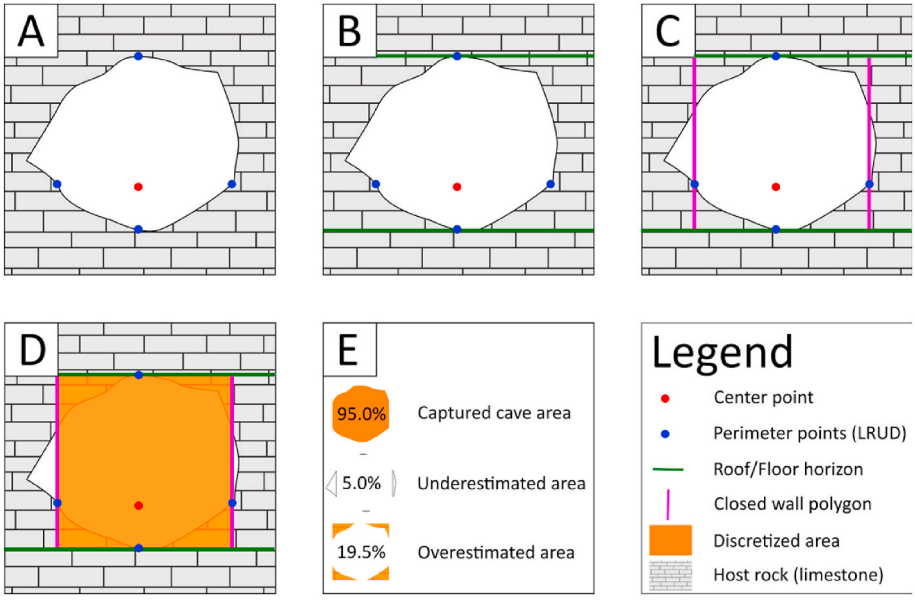

Fig. 4. Method 2 - Cross-sectional conceptual illustration of the workflow suggested by Ledsaak (2016). A) Cave survey data containing center-point (red dot) and LRUD (blue dots) is used as input to reservoir modelling software B) Roof- and floor horizons (green line) are constructed based on the up- and down points, respectively. The horizons constrain the vertical extent of the cave. C) Wall points (L and R) are used to generate a closed polygon (pink lines) used to constrain the lateral extent of the cave. D) The final discretized area representing the gridded cave (orange square). E) Area coverage: area calculations (image analysis from the illustration) show that for this example 95.0% of the original cave area is discretized by this method. However, based on the illustration, the method fails to discretize 5.0% of the original cave and overestimate the total area by 14.5%. (For interpretation of the references to colour in this figure legend, the reader is referred to the Web version of this article.)

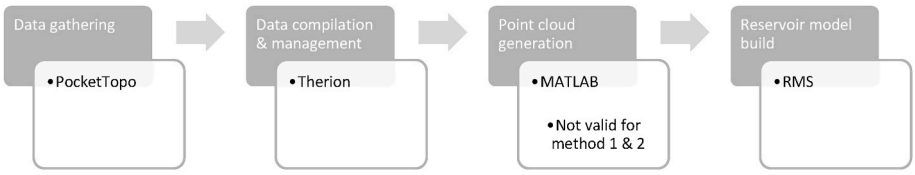

Fig. 5. Workflow steps (grey) and associated software (white) - from data collection to reservoir model build. The key aspect here is utilisation of a point cloud to discretize the cave network at higher resolution. In all cases alternative software could be employed to individual tasks.

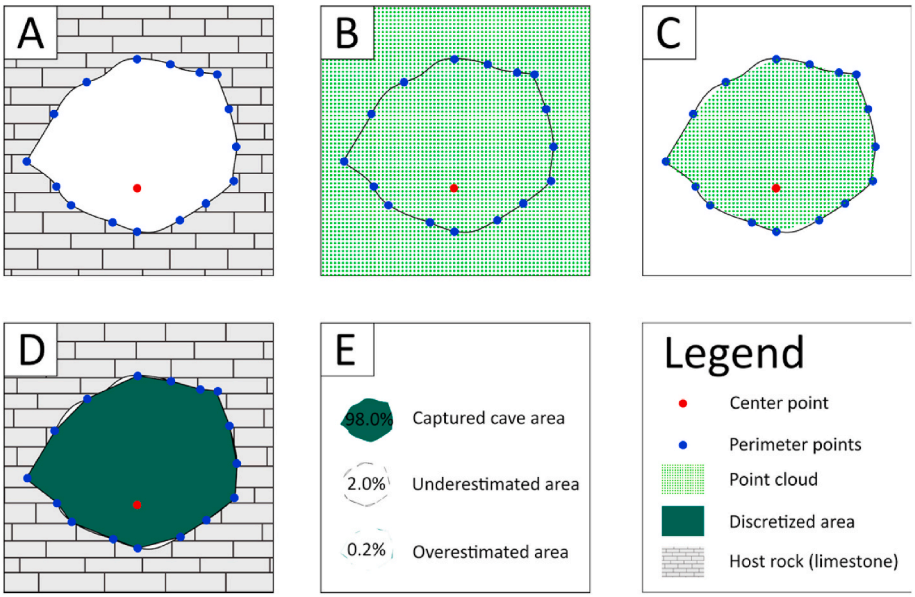

Fig. 6. Method 3 - Cross-sectional conceptual illustration of the workflow. A) Cave survey data containing centre-point (red dot) and wall shots (blue dots) is used as input into MATLAB. B) A defined volume of dense equally spaced points, representing the modelling domain, is generated in MATLAB. C) A predefined MATLAB code is used to discretize points inside the cave system, subsequently generating a *.csv file containing X, Y, Z -values for each point within the cave area. Note that the software discretizes the point cloud by drawing straight lines between the perimeter points. D) The dense point cloud representing the cave system is then imported into RMS and run through geometric modelling (calculating distance from object/point), subsequently filtering and discretizing the data. E) Area coverage: area calculations (image analysis from the illustration) show that for this example 98.0% of the original cave area is discretized by this method. However, based on the illustration, the method fails to discretize 2.0% of the original cave and underestimate the total area by 1.8%. However, volumetric over- or underestimation of the gridded volume should be expected when "forcing" a complex geometric shape into a gridded framework. The magnitude of which will be determined by a combination of the applied global grid cell resolution, point cloud density and applied filter cut-off. (For interpretation of the references to colour in this figure legend, the reader is referred to the Web version of this article.)

calculating "distance to object" parameter, the objects here being the points along the skeleton line segments. A filter function is then used to create a parameter rendering the "cave" as a string of cells with their centre-point at a given distance from the skeleton line (Fig. 3), defining a "filtered distance" hereafter referred to as cut-off or cut-off value. In this study, the estimated average conduit radius of 6 m (estimated mean roof height from the cave survey of the master conduit and two tributaries) is used as a cut-off. When employing a high grid resolution, Method 1 renders the cave passages as having a circular cross-section with a fixed and constant diameter (Fig. 3C). At lower grid resolutions, cross-sections will have a "blockier" appearance.

3.3. Method 2

Method 2 (Ledsaak, 2016) uses a four-step workflow (Fig. 4) and cave survey data in LRUD format (left-, right-, up- and down-points) in addition to the survey station positions employed in Method 1. The LRUD survey data is imported into RMS™ as points for each group; wall, roof and floor. For geometrically simple karst systems, such as single-tiered systems, the floor- and roof points are then used to generate bounding horizons, constraining the vertical extent of the cave. A new closed wall polygon is generated by manually tracing the wall points, which constrains the lateral extent of the cave. In the gridded model, the roof- and floor horizons and the closed wall polygon are then used to delimit the cave. In geometrically complex and multi-tiered cave systems, using this approach becomes a bit more demanding, as the horizons defining the roof and floor exist at multiple stratigraphic levels with overlapping XY positions which cannot be mapped as a single, continuous surface. As the software does not allow for stratigraphic zones crosscutting other zones, the surfaces and polygons must be grouped according to cave tier. In these cases, the wall polygons must be split into several segments for each cave tier, and subsequently merged into a single polygon. Horizon mapping must be carried out for each roof and floor polygon, and new surfaces generated. Finally, the cave must be gridded for each cave tier, constrained by the associated boundary surface and wall polygon, before merged into a single grid model.

3.4. Method 3

The new approach, Method 3, consists of a four-step workflow summarized in Figs. 5 and 6.

First, cave survey data, comprising spatial data of survey-station positions- and multiple wall points, is gathered using modern equipment and techniques (Fig. 6A). Collected data is imported into a cave survey data management software (Therion) to generate a 3D cave model and subsequently exported as X-, Y-, and Z-points. The entire modelling domain is then densely populated with equally spaced geo-referenced points in MATLAB (Fig. 6B), where an algorithm is used to discretize the cave volume and thus remove all points outside the cave boundary. This produces a dense point cloud representing the cave system (Fig. 6C). The MATLAB-generated geo-referenced points are then imported into RMS, and a new continuous parameter, representing the

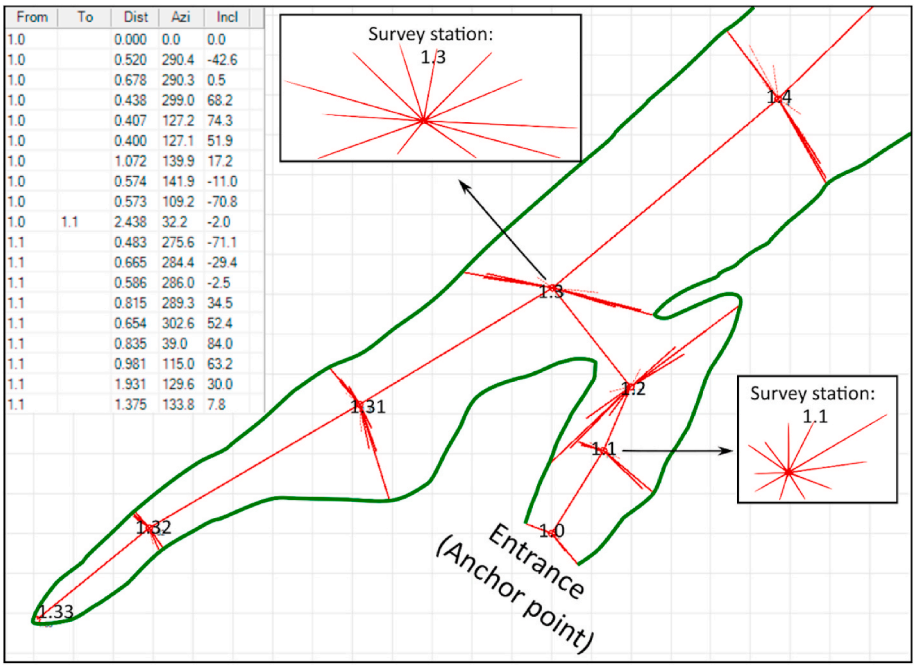

Fig. 7. Layout example of cave survey data in PocketTopo. Left: cave survey data showing station number (from and to), distance (m), azimuth (°) and inclination (°) of each shot. Right: Data visualization (red) in real-time allowing manual sketching (green line). Inserts show cross-section for survey station 1.1 and 1.3. (For interpretation of the references to colour in this figure legend, the reader is referred to the Web version of this article.)

distance to the points, is generated by geometric modelling; following the same workflow as Method 1. The cave system is then discretized by filtering the continuous parameter (Fig. 6D).

3.5. Software

PocketTopo is an application that receives and stores cave measurements (station number, distance, azimuth and inclination) directly from a laser rangefinder. The software allows managing survey data, reference points and trip information, and includes the possibility of freehand sketching between survey stations (e.g. green line in Fig. 7).

Therion is an open-source software for survey data processing. The software is used to compile cave surveys and for geo-referenced survey anchoring, loop-closure, map generation, 3D cave modelling and more (Budaj and Mudrák, 2008). In our proposed method, the survey data from PocketTopo (e.g. Fig. 7) is imported into Therion to generate a geo-referenced 3D model. The wall boundaries of the model are then exported as a *.txt file comprising X-, Y-, and Z-points.

In MATLAB, the modelling domain is densely populated with equally spaced, geo-referenced points. The wall periphery data, from Therion, are then imported and used to constrain the cave system by eliminating all points outside the cave. The remaining geo-referenced points now provide a point-cloud rendering of the cave system. These points can then be exported as a comma-delimited text file (*.csv). In this study, point clouds with two different point densities were constructed: 0.5m and 1m. Unless stated otherwise, all following models, graphs, and

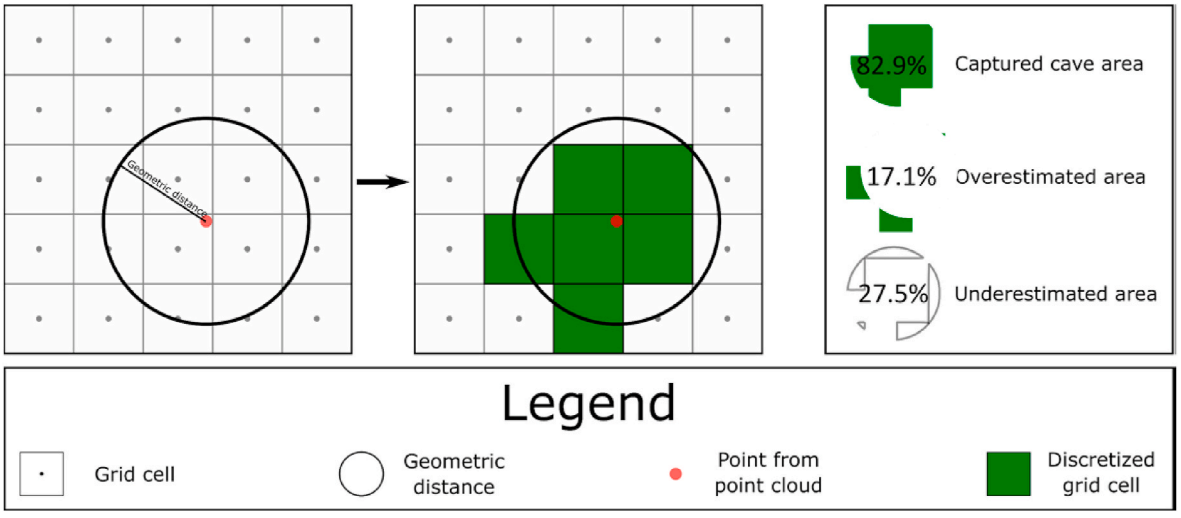

Fig. 8. 2D conceptual illustration of geometric modelling and associated geometric distance function. The built-in RMS™ function generates a continuous parameter with parameter values representing the geometric distance from an object, in this case, points. The parameter can be filtered, and a desired cut-off value can be applied to constrain a volume. Area coverage: area calculations (image analysis from the illustration) show that for this example 82.9% of the original cave area is discretized. Note that the illustration is in 2D, whereas the geometric distance is a 3D calculation.

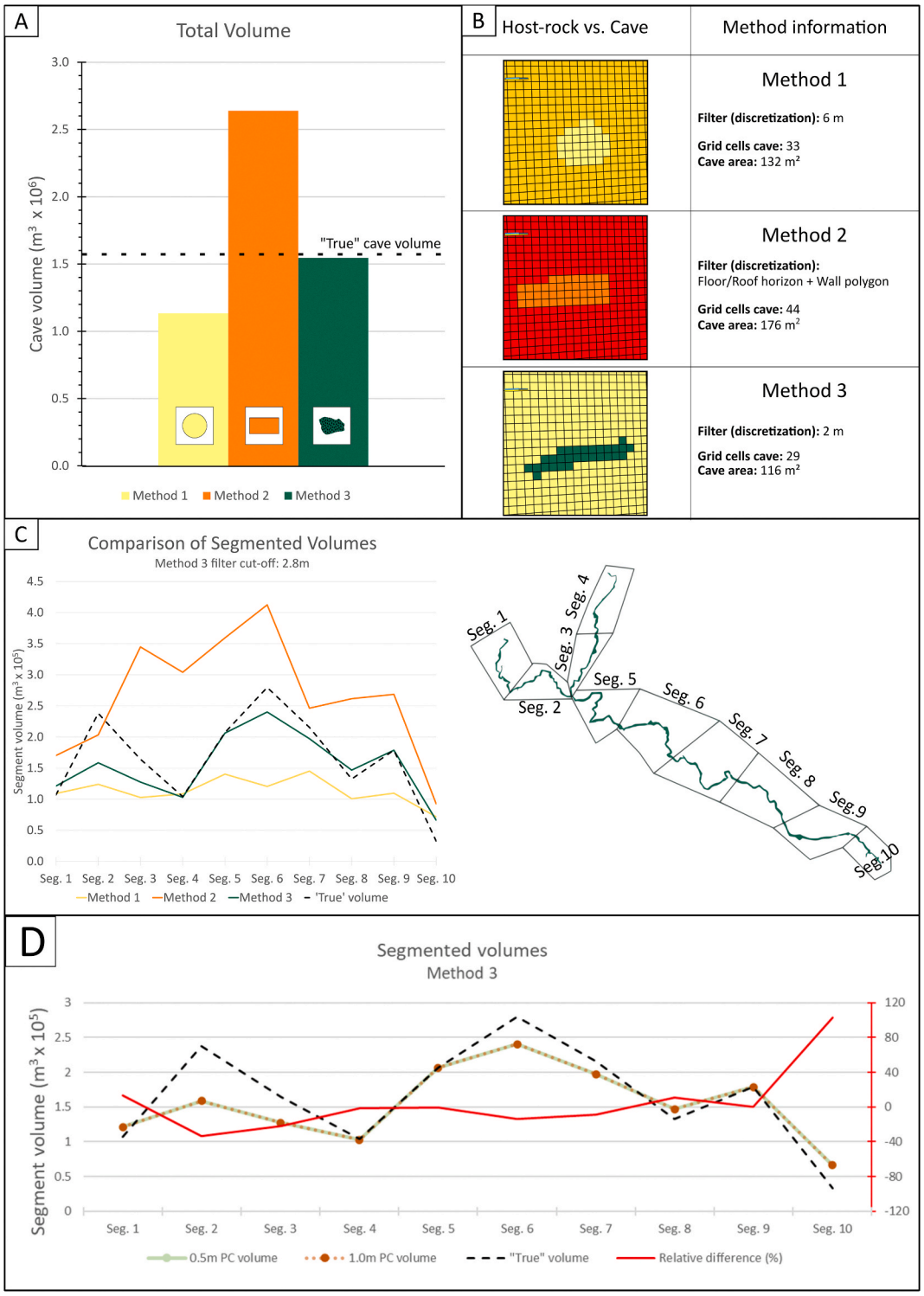

Fig. 9. A volumetric comparison of studied methods. All graphs represent a global grid resolution of 2 × 2 × 2m. A) Histogram showing the difference in total volumetric representation between the methods benchmarked against the "true" cave volume. B) Cross-sectional example of the gridded end-result of each method. Note that the angle of view and section are identical for all models. C) A volumetric comparison for 10 different segments (as marked on the cave plan) of the resulting grid models. D) The relative difference between Method 3 and the "true" cave volume. Segmented volumes rendered using two different point cloud densities (0.5 and 1-m spacing) show that the volumetric rendering is identical using different point cloud densities. Colour coding used for the different methods: Method 1 = Yellow, Method 2 = Orange, and Method 3 = Green are consistent with all following grids, charts, and graphs. (For interpretation of the references to colour in this figure legend, the reader is referred to the Web version of this article.)

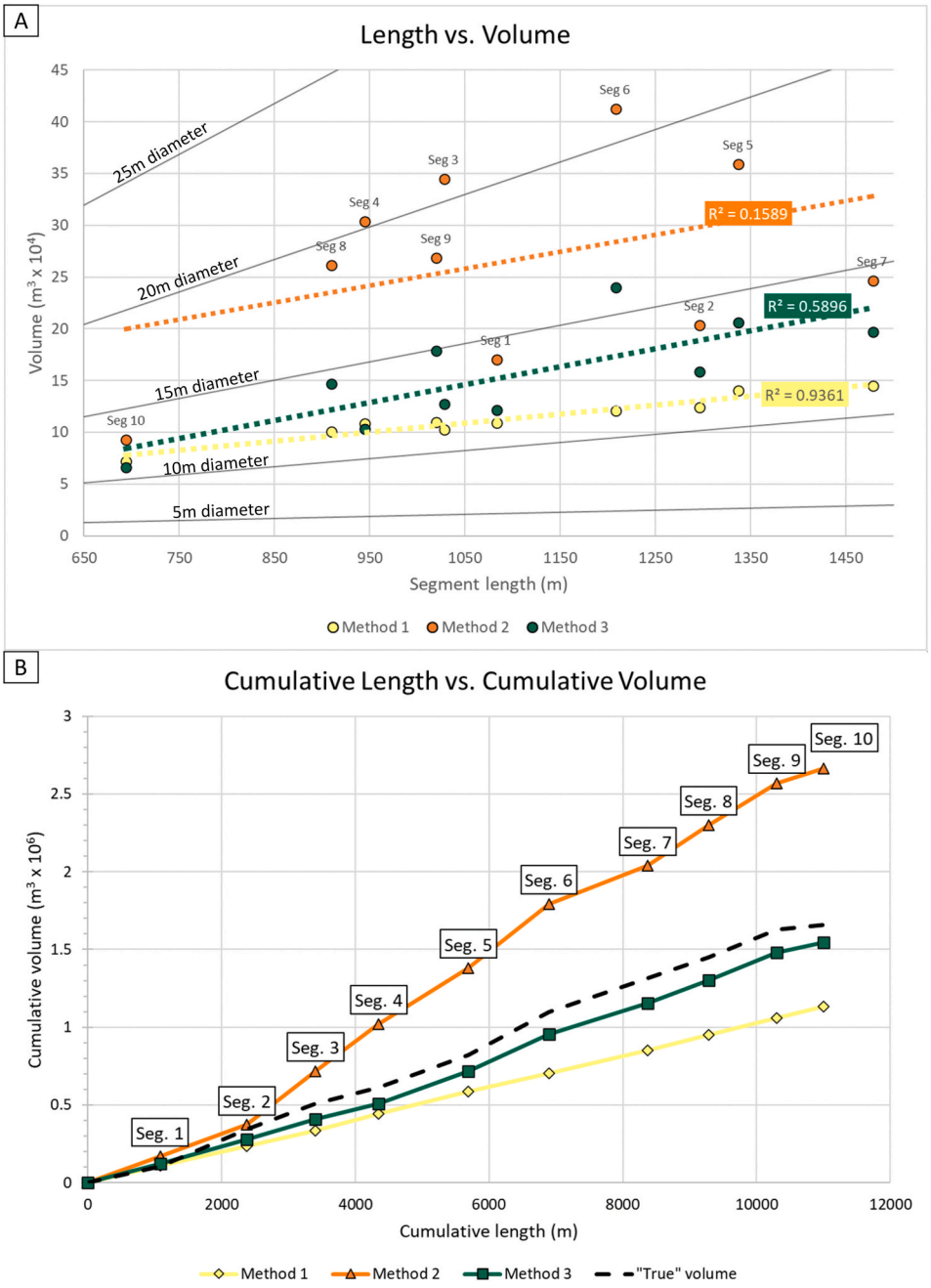

Fig. 10. Comparison of cave volume over passage length for different estimation methods for models using a global grid resolution of 2 × 2 × 2m. Method 1 is discretized by a filter cut-off of 6m, Method 2 by bounding horizons and a closed polygon, and Method 3 by a filter cut-off of 2.8m. A) Segment length vs volume. For comparison, grey contour lines show volume of cylinders with constant diameters. B) Cumulative length vs cumulative volume - Segments 1 to 10. Note the excellent correlation between the "true" volume and Method 3 in B) and that Method 1, as expected, results in a linear graph due to the uniform cylindrical rendering of the cave system.

illustrations refer to results from the 0.5m (X,Y,Z) point cloud.

The industry-standard reservoir modelling software RMS™ 11.0.1 is used to generate a gridded model of the cave system. Geo-referenced points (MATLAB generated *.csv file) representing the cave system are imported into RMS using the custom format function. In the custom settings, data headers are removed, and data treated as a single object with comma-separated columns. Note that it is important that the coordinate system used in previous steps is consistent with the one used in RMS. Even though correct global positioning is not required for a given study, significant decimal places vary between different coordinate systems (i.e. geographic coordinate system vs projected), which may cause import problems. The cave system now comprises a dense 3D point cloud. The point cloud can be used in pre-established gridded reservoir models or a new grid with appropriate grid parameters. The cave system is discretized using the built-in RMS parameter utility "*Geometric modelling*" and the associated "*Distance to objects*" function (Fig. 8). This function generates a continuous parameter with cell parameter values representing the distance from the objects, which in this case are the points within the cave. A new grid with discrete parameter values is then created to discretize the cave system. The cave system is discretized by using "*parameter utilities*" and the "*calculator*" function with the following equation (1):

IF "continuous geometric modelling parameter"⩽"cut
– off value" THEN "new discrete parameter"
= "desired parameter value" ENDIF (1)

In this study, the applied parameter names and cut-off values are used (2):

$$IF\ Geometric \leq 2\ THEN\ CaveNoCave = 1\ ENDIF \quad (2)$$

Here, an empirical cut-off value of 2m was applied to all models.

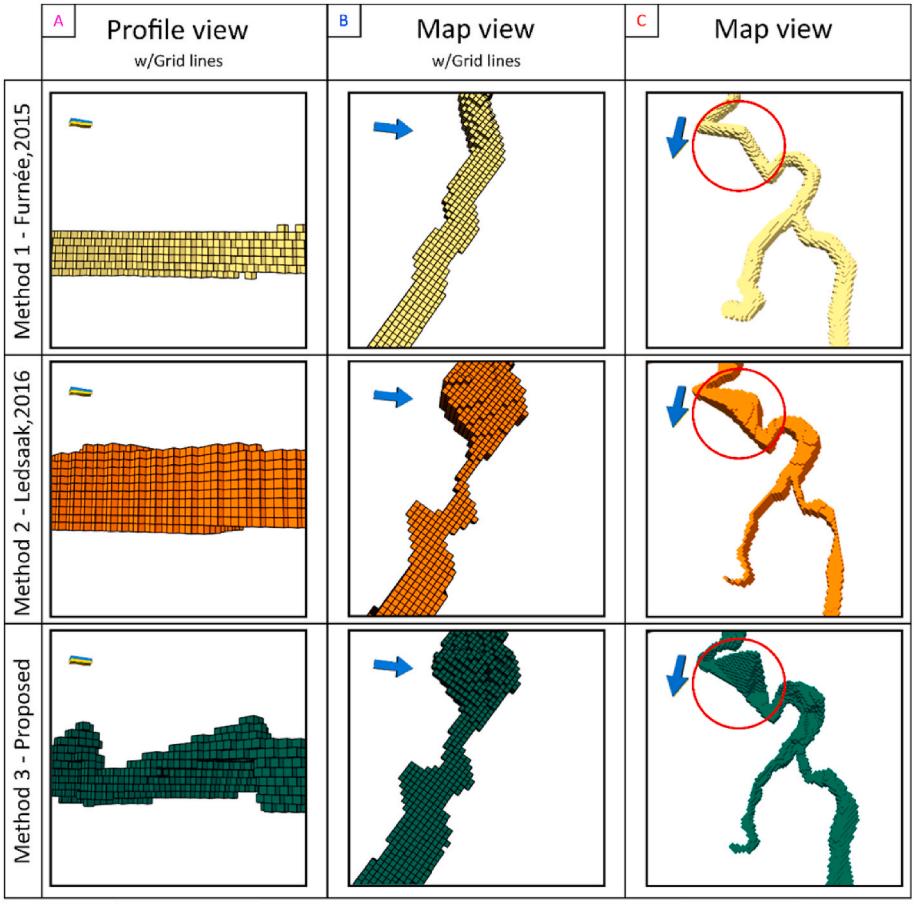

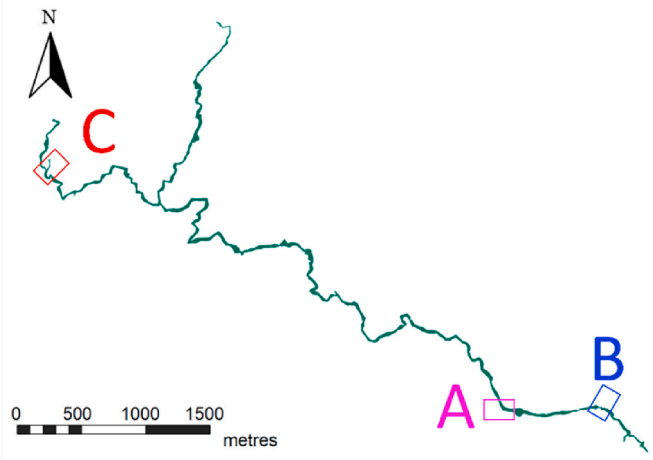

Fig. 11. Grid model comparison using various methods. All models in the same column show the same section, with an identical scale and angle of view. 3D close-up views show significant volumetric and geometric differences between the three methods. A) Profile view showing an apparent lack of geometric resolution in Method 1 and 2. Both methods fail to capture the looping morphology of the roof evident in Method 3. B) Map view showing, as expected, that Method 1 fails to capture abrupt conduit narrowing and widening, which are seen clearly in using both Method 2 and 3 that seem to provide good geometric representations of the cave system. However, in the narrow passage section Method 2 generates a lower volume compared to Method 3, with the difference likely relating to the input data used in Method 2. This method only utilizes only a single point for each wall to delineate the lateral extent of the cave and thus the modelling result is highly dependent on the spatial arrangement of the survey station or selected wall shots (e.g. as illustrated in Fig. 18). C) Map view of an area where a tributary joins between the western branch to the main conduit. All three methods ensure grid cell connectivity between the tributaries but result in significantly different geometric- and volumetric representations. The apparent looping conduit morphology in the southern part of model generated using Method 1 (red circle), clearly shows that this modelling approach may introduce morphological artifacts. It is clear from Methods 2 and 3 (red circles) that this is an area with elevated cave roof heights, and that the apparent looping morphology in Method 1 is a result of the spatial arrangement of the survey station. North direction in gridded models indicated by a blue arrow. (For interpretation of the references to colour in this figure legend, the reader is referred to the Web version of this article.)

Note that cut-off values used to discretize the cave system in the gridded model should be carefully selected and adjusted to fit grid- and point cloud resolution.

3.6. Volumetric estimation

In order to evaluate the volumetric accuracy of each method, grid volumes must be benchmarked against the best estimate of cave volume. In this study, an estimated cave volume is calculated by extrapolating the cross-sectional area between the survey stations. First, to calculate the area, the cave survey data must be transformed into vectors with coordinates (x_n, y_n) in a cartesian coordinate system. Then, the area can be calculated using equation (3) for planar non-self-intersecting polygons (Weisstein, 2020):

$$A = \frac{1}{2}\left(\begin{vmatrix} x_1 & x_2 \\ y_1 & y_2 \end{vmatrix} + \begin{vmatrix} x_2 & x_3 \\ y_2 & y_3 \end{vmatrix} + \ldots \begin{vmatrix} x_n & x_1 \\ y_n & y_1 \end{vmatrix}\right) \quad (3)$$

The cross-sectional area of each survey station is then multiplied by the distance to the consecutive station to get an estimated volume for each segment. Finally, all segments are summed to get an estimated total cave volume, hereafter referred to as the "true" cave volume. In order to ensure all cross-sections comprise non-self-intersecting polygons, a manual quality check was carried out for each survey station accompanied by data rearrangement.

4. Results

The Maaras cave survey was split into ten approximately equal

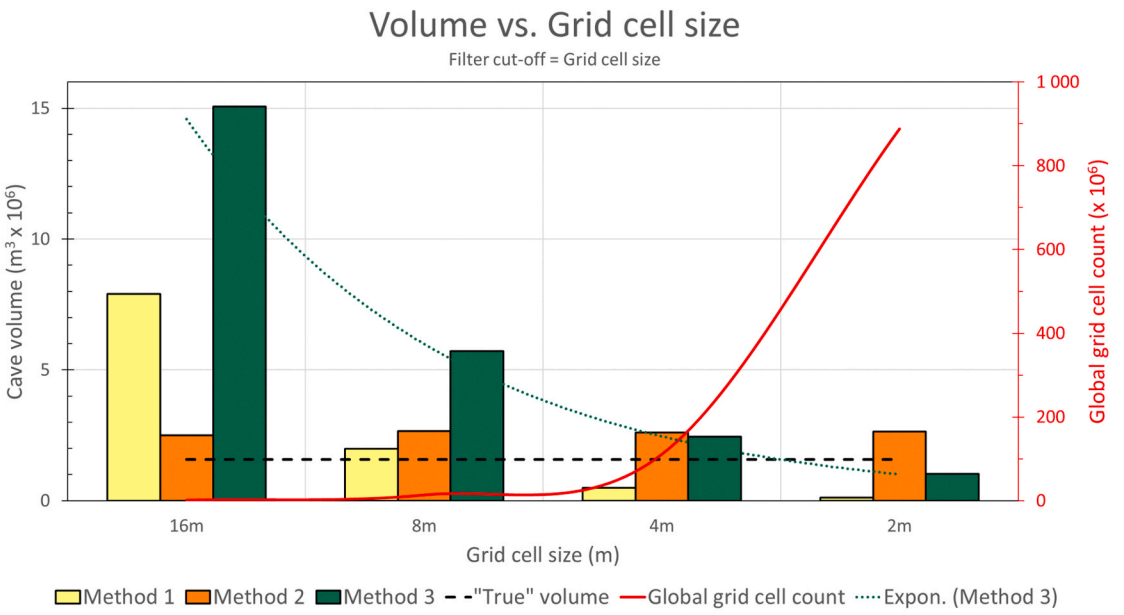

Grid cell resolution vs. filter cut-off

		Grid cell resolution 16m				Grid cell resolution 8m				Grid cell resolution 4m				Grid cell resolution 2m			
Filter cut-off (m)		2	4	8	16	2	4	8	16	2	4	8	16	2	4	8	16
Total volume (Mm^3)	Method 1	0.08	0.36	1.71	7.91	0.12	0.51	1.99	8.01	0.11	0.50	2.02	8.07	0.12	0.50	2.02	8.06
	Method 2	2.51				2.66				2.61				2.66			
	Method 3	0.84	2.04	5.24	15.07	1.10	2.39	5.72	15.34	1.11	2.45	5.84	15.55	1.03	2.38	5.73	15.40

Fig. 12. Variation in total volumetric representation by different methods, grid cell resolutions (X = Y = Z) and filter cut-off values. Tabulated total volumes are in most cases larger than the "true" cave volume of 1.58 Mm^3. Crossed-out cells in the table indicate geocellular rendering lacking complete cell interlinkage throughout the cave system. Note that Method 2 discretize the cave system by bounding horizons and closed polygons and thus the filter cut-off will not apply to this method.

segments, with main passage lengths of 1100m ± 220 (mean ± SD) (Figs. 9C and 10). Results are presented for three separate model versions of each segment generated using Methods 1, 2 and 3. Global grid resolution was kept identical for all models (2 × 2 × 2m) to allow comparison. If not specified otherwise in the graphs or illustrations, the cave system was discretized using a filter cut-off distance of 6 m in Method 1, a combination of bounding horizons and a closed wall polygon in Method 2, and a filter cut-off distance of 2.8 m for Method 3. At this grid resolution and associated boundary conditions, all three methods capture the orientation and connectivity of the cave conduits (Fig. 11), but geometric rendering differs significantly (e.g. Figs. 9B and 11). This is highlighted when comparing calculated cavity volumes from the three grid model versions with the "true" 3D volume from the survey data. The total volume yielded by Method 1 is 1.13 Mm^3 (assuming a mean conduit diameter of 12 m), which is less than half the total volume of 2.66 Mm^3 yielded by Method 2 (Fig. 9A). Both estimates are significantly different from the "true" cave volume of 1.58 Mm^3, with Method 1 resulting in an underestimate (relative difference of 33%) and Method 2 an overestimate (relative difference of 51%). The volumetric estimate yielded by Method 3 is 1.55 Mm^3 which is within 2% of the estimated "true" cave volume.

Considering individual segments, models generated using Method 2 consistently overestimate the cave volume (in all segments except in Segment 2) when compared to models built by using Method 1 and 3 (Fig. 9C). The latter two provide comparable volumes in some segments (notably the upper sections of both branches of the cave), but show a significant volumetric deviation in all but the last segment in the main passage downstream of the confluence of the western and eastern branches (segments 5, 6, 7, 8 and 9; Figs. 9C and 15).

In order to investigate the impact of grid cell resolution and applied filter cut-off values, a series of models were built using different grid cell dimensions and filter cut-off values equalling associated grid cell sizes: 16m, 8m, 4m, and 2m (Fig. 12). Due to CPU constraints, the highest practical grid resolution tested was 2 × 2 × 2m, which resulted in a global grid with ~9 × 10^8 grid cells.

For Method 3, the relationships between volumetric representation and applied cut-off values were plotted for different grid cell resolution, to identify potential interlinkage between model set-up and resulting volumetric rendering (Fig. 13A). Similarly, multiple segments (only two presented in this article) were appraised to confirm these trends (Fig. 13B and C). The full geocellular cave model and all segmented models show a clear polynomial trend (coefficient of determination R^2 of 1), for a given grid cell resolution, between the filter cut-off value and resulting volumetric rendering (Fig. 13).

A visual evaluation of cell-to-cell interlinkage (Fig. 12) show that Method 1 renders all grid models with a cut-off value less than the grid cell resolution incoherent. For Method 2, only a grid cell resolution of 2 × 2 × 2m provides interconnected cave grid cells, whereas all other grid cell resolutions result in disconnected cave grid cells. Method 3 provides the best grid cell coherency with most grid cells resolutions and filter

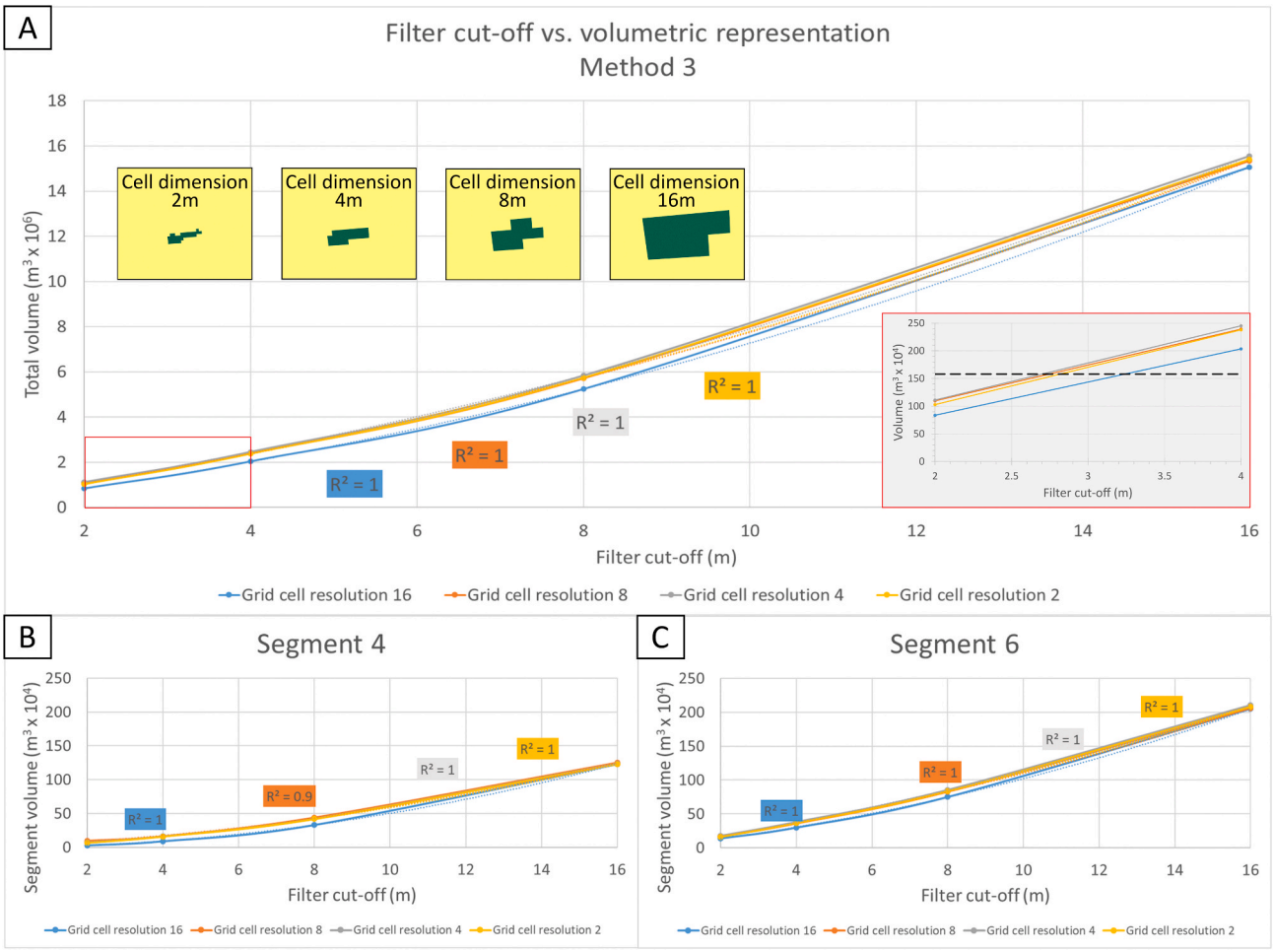

Fig. 13. Volumetric rendering at various grid cell resolutions and applied filter cut-off values. A) Volumetric rendering of the complete grid model. Insert: close-up (red square) of cut-off value ranges that give volumes close to the "true" cave volume (black line). Yellow boxes: Cross-sectional view of a cave corridor at different grid cell resolutions (X = Y = Z). The filter cut-off (2m) and angle of view is identical for all boxes. The trend lines show an evident polynomial trend (coefficient of determination (R^2) of 1) between volumetric rendering, grid cell resolution, and filter cut-off values. B) Volumetric rendering of segment 4 (Fig. 15). C) Volumetric rendering of Segment 6 (Fig. 15). Note the clear polynomial relationship between filter cut-off and resulting volumetric rendering in all graphs. Grid cell resolution has a minor impact on the volumetric rendering for values of 8 m^3 or lower, but at 16 m^3, the rendered volume is reduced by 19–25% using a filter cut-off of 2m. (For interpretation of the references to colour in this figure legend, the reader is referred to the Web version of this article.)

cut-off values resulting in coherent cave models. However, at coarser grid cell resolutions and low cut-off values, also Method 3 failed to render a continuous cave model (e.g. Figs. 12 and 14).

5. Discussion

The results show that although all methods are applied to the same cave survey data, the volumetric and geometric representations of the cave system in the geocellular model will differ depending on the algorithm used. Method 3, apparently provides a better geometric description of the cave system compared to the two other methods (Figs. 6 and 11). However, the modelled volume in all methods deviates from the benchmarked volume (1.13, 1.55 and 2.66 Mm^3 for Method 1, 3 and 2, respectively, compared to a "true" volume of 1.58 Mm^3). This could suggest that the volumetric representations of the grid models reflect a combination of the resolution and availability of input data, the modelling approach and the grid model set-up (grid resolution). Method 3, with optimal cut-off value, results in a volumetric rendering close to that of the "true" volume from the cave survey. Nevertheless, it is crucial to keep in mind that the "true" volume is most likely an underestimation, as the wall shots only represent the distance to the closest obstacle (e.g. Fig. 16). Also, many karst caverns are inaccessible for humans as they are either too small to access or infilled/blocked by clastic sediments, adding to the volumetric underestimation. The uncertainty in karst pore volume can be evaluated using fractal distributions (e.g. Curl, 1986; Pardo-Igúzquiza et al., 2018) and sedimentary thickness mapping (e.g. Lønøy et al., 2019a), and can thus be included in a reservoir model using stochastic modelling. However, this is outside the scope of this study but shows that it is difficult to establish the actual volume of a karst system and that several factors need to be considered in paleokarst reservoir modelling.

A well-known challenge in reservoir modelling is accurate and efficient modelling of complex morphologies using corner-point- or pillar-based unstructured grids (e.g. Branets et al., 2009; Mallison et al., 2014). Rendering irregular 3D shapes as geocellular bodies at a given cell size resolution will cause over- or underestimation of body volumes (Fig. 17). Even an optimal fine-tuning of the cut-off value for the "distance to objects" calculation will cause grid cell corners either to extrude beyond the periphery or fail to precisely fill in the detailed shape of the actual mapped body.

5.1. Method 1

Method 1 proved to be a time- and CPU efficient method for incorporating cave survey data into industry-standard reservoir modelling tools (Table 1). The method relies on simple datasets that might be easy

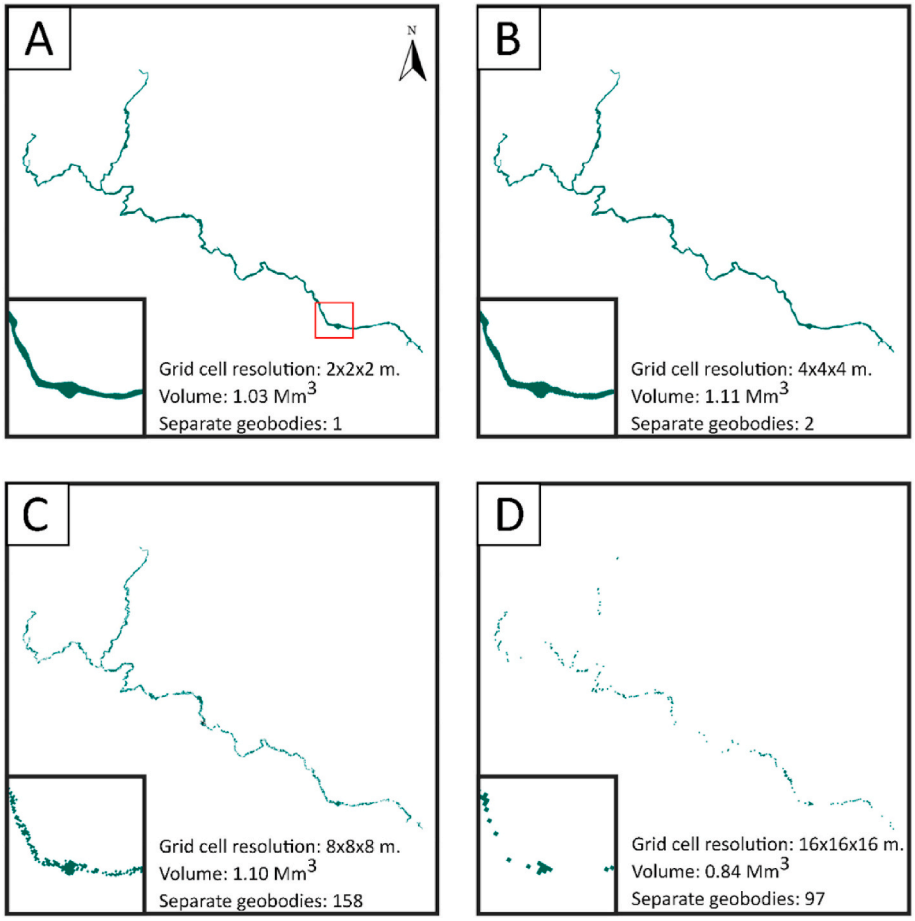

Fig. 14. Geocellular rendering at different grid cell resolution using Method 3. Filter cut-off value is kept constant at 2m for all models. Inserts show a close-up view of a section of Segment 9 (highlighted with a red square) in the same area of each model. Separate geobodies determined by image analysis. A) Grid cell resolution (2 × 2 × 2 m) equal to the cut-off value. Volumetric representation close to the "true" volume. B) Grid cell resolution (4 × 4 × 4 m) equals twice the cut-off value. Volumetric representation close to the "true" volume. C) Grid cell resolution (8 × 8 × 8 m) equals four times the cut-off value. Volumetric representation close to the "true" volume. Diminishing cell-to-cell connectivity. D) Grid cell resolution (16 × 16 × 16 m) equals eight times the cut-off value. Volume underestimated by a factor of 1.39 and cell interlinkage lost. Note that separate geobodies significantly increase when grid cell resolution increase from 4 m^3 to 8 m^3. However, in a paleokarst setting, the collapse footprint may subsume these isolated geobodies and create a coherent fluid environment if the geobodies separation distance is less than the lateral collapse propagation. (For interpretation of the references to colour in this figure legend, the reader is referred to the Web version of this article.)

and quick to collect. However, the resulting grid model lacks morphological heterogeneities often associated with karst systems, such as abrupt conduit narrowing/widening and irregular roofs and floors (Figs. 3, 9B and 11 and 15). Conduits formed along stratigraphic horizons and along fractures are expected to have different geometries (wide and low vs tall and narrow) and sedimentary infill. The nature of infill type is closely related to the local hydraulic regime, cavity breakdown and diagenesis. These factors ultimately control fluid flow. As Method 1 render all cave corridors as cylinders with a fixed and constant diameter, the method will probably work better for conduits with a circular to elliptical cross-sectional shape (e.g. phreatic conduits with low fracture density formed in homogenous limestones). Method 1 may also create morphological artifacts (e.g. Fig. 11C) as the vertical and horizontal extent of the conduit is only constrained by a fixed distance to a single reference point.

Studies have shown that some karst voids and conduit sections may remain open at great depths up to 6 km (e.g. Loucks (1999); Lu et al. (2017)). Synthetic conduits with a uniform circular geometry may prove unsuitable for establishing rules for subsequent delimited forward collapse modelling, as it would make morphological identification of cave sections prone to roof collapse difficult. Attic pockets acting as hydrocarbon traps may thus be overlooked or have an uncertain spatial distribution in the final grid model; potentially resulting in imprecise estimates of stock-tank oil original in place (STOOIP) and gas initially in place (GIIP) and probably an overestimation of recovery. Moreover, the volumetric accuracy of the resulting grid models reflects the morphological complexity of the cave system in addition to the selected cut-off value constraining the vertical- and horizontal extent of the conduits (Figs. 10, Figs. 12 and 15). In most cases, except maybe in wet caves, cave surveys comprise at least some boundary measurements (minimum LRUD). Thus, this method may prove to be oversimplified or obsolete for most cave survey data.

5.2. *Method 2*

Method 2 also proved to be a time- and CPU efficient method for reservoir modelling of single-tiered cave systems with simple morphology, such as Maaras (Table 1). However, studies by Ledsaak (2016) showed that, using existing industrial reservoir modelling tools, the method is intricate and time-consuming when used for multi-tiered caves with complex geometries. Method 2 captures the orientation and connectivity of the conduit and provides a better geometric approximation of the real cave morphology than Method 1 (Figs. 9B and 11). Still, Method 2 only relies on four points (for each survey station) delimiting the vertical and horizontal extent of the cave system. Thus the gridded cross-sections will comprise extrapolated rectangular shapes between stations (e.g. Fig. 9B).

In the present study, the models generated using Method 2 overestimate the total cave volume in all segments except Seg 2 (Fig. 9C). A volumetric deviation is expected as Method 2 renders all cave passages as rectangles (e.g. Figs. 4 and 18). However, the volumetric overestimation could be related to the input data. The Maaras cave survey was conducted using contemporary surveying techniques (Fig. 2B) and included multiple wall shots. In the absence of fixed LRUD points, these had to be generated from the measured wall shots by an automatic vector interpolation function in Visual Topo (2017). Following Method 2, the grid model will always comprise volumes that are either too large or small, depending on the cave survey array (e.g. the spatial distribution of the survey station relative to the conduit size and shape in Fig. 18). Although a volumetric deviation is expected, the volumetric

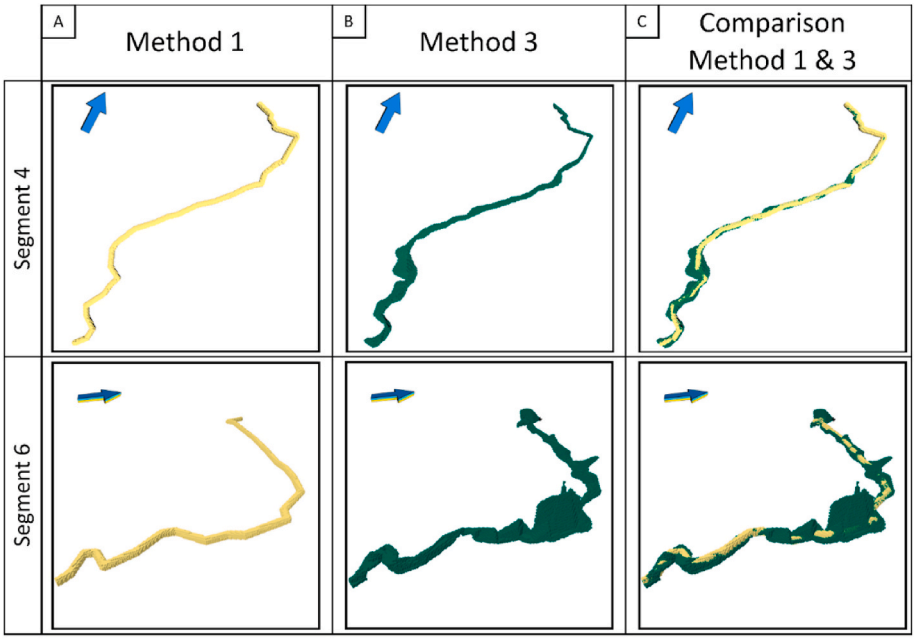

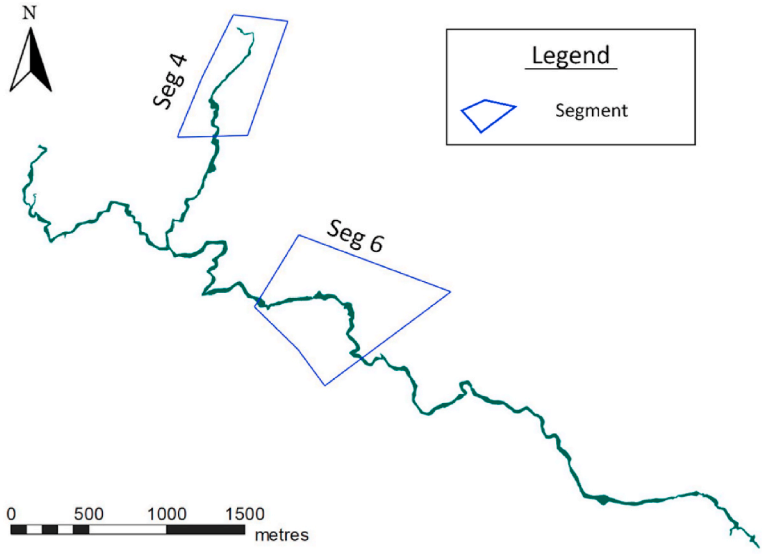

Fig. 15. Segmented grid model comparison. A) Grid model of segment 4 and 6 using Method 1. B) The same segments using Method 3. C) Grid model comparison between Method 1 and 3 with identical segmentation and angle of view. Areas shown in yellow are those where the cave predicted by the cylindrical model exceeds the volume from Method 3, whilst the green areas are areas where Model 1 underpredicts the magnitude of the passage. Note that the biggest volumetric difference (Seg 6) is in an area with a heterogeneous cave morphology, large chambers and associated high abundance of break-down related breccias (Lønøy et al., 2019a). North direction in gridded models indicated by a blue arrow. (For interpretation of the references to colour in this figure legend, the reader is referred to the Web version of this article.)

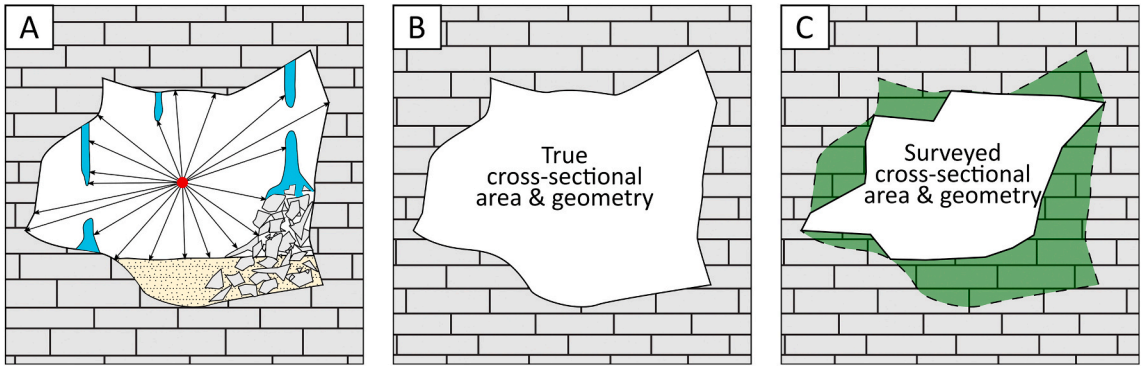

Fig. 16. Method 3 - Example of a potential coverage area using modern cave survey techniques. A) Conventional survey set-up and associated directional shots. Note that the shots only measure the distance, inclination, and azimuth to the closest obstacle (i.e. stalactites, stalagmites, breccia cones and clastic sedimentary infill). B) The true cross-sectional area and geometry (black line). C) The cross-sectional area and geometry covered by the cave survey (black line) and the true area and geometry (green area). (For interpretation of the references to colour in this figure legend, the reader is referred to the Web version of this article.)

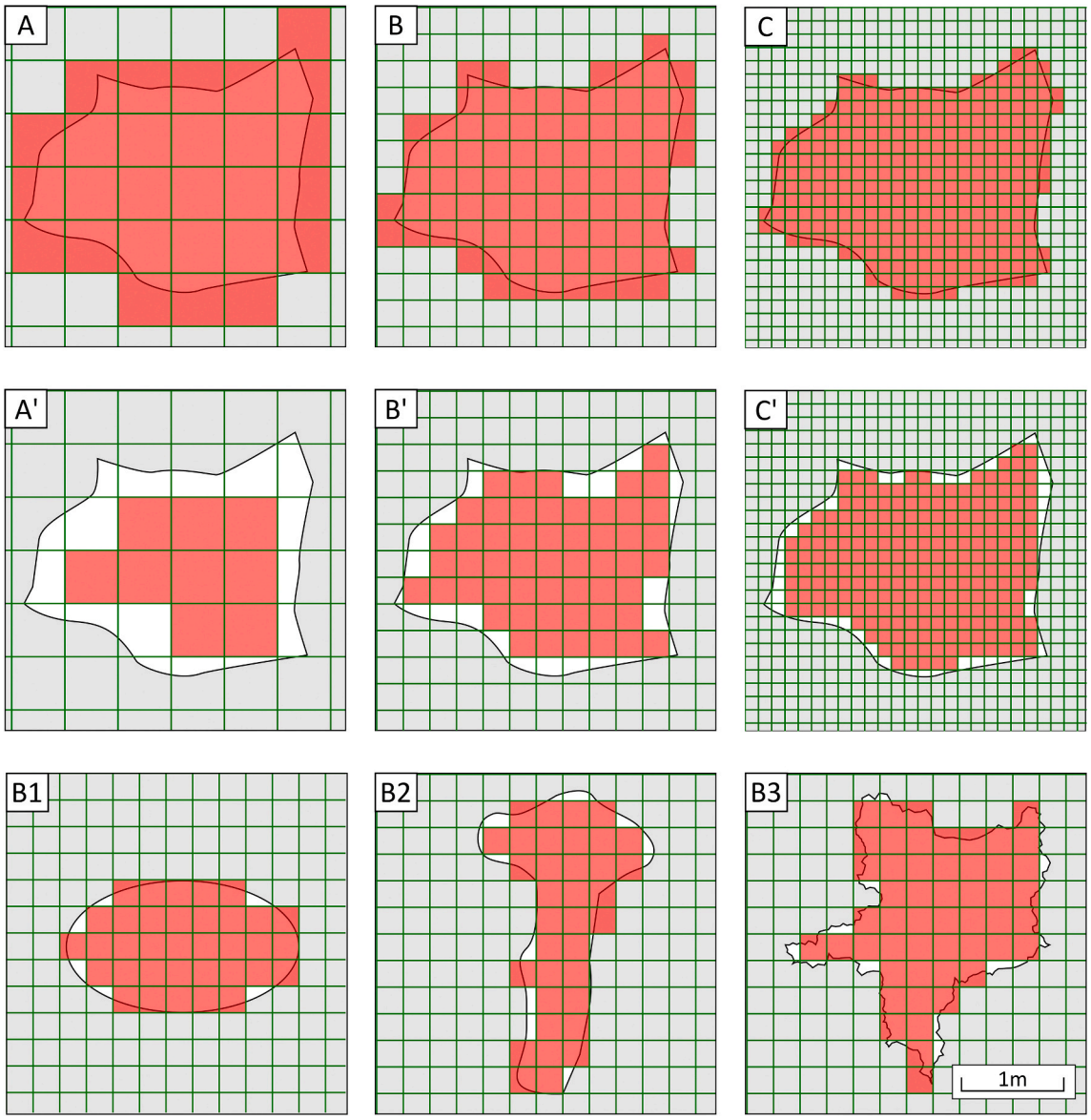

Fig. 17. Discretized area by different global grid resolutions. Note that this figure is only for illustrative purposes and that a reservoir modelling software could discretize the cave area differently. The grid cell size in this illustration is relative, and thus a unit of measure is not applied. A–C: Grid cells completely encompassing the cave perimeter. A′-C': Grid cells kept within the cave perimeter. B1–B3: Geocellular rendering of different passage shapes: phreatic conduit, vadose canyon and complex passage geometry with asperities. Grid cells kept within cave perimeter. A) Large grid cells - size 1. B) Intermediate grid cells – size 1/4. C) Small grid cells – size 1/16. As the grid framework becomes finer, the morphological resolution increases. Note that depending on whether grid cells encompass (A–C) or are kept inside the cave perimeter (A′-C′), volumetric rendering respectively decreases or increases with finer grid resolutions.

error using automatically generated LRUD points may be larger than those derived from grid models generated using reliable LRUD survey data. This inaccuracy of using LRUD data generated from multiple wall shots becomes evident in Segment 2, where there are an obvious error in the generated roof (U) and floor (D) points. In this segment, some of the floor points (D) has a higher elevation than the roof points (D) and thus the floor- and roof horizons are crossing resulting in non-discretized areas which could explain the volumetric underestimation shown in Fig. 9C.

5.3. Method 3

Method 3 involves a few additional steps and software combinations compared to the two other methods. Most of these steps are fully automated and do not require significant manual effort. In terms of time-consumption and complexity, our new method is significantly quicker and easier than Method 2, but not as fast and easy as Method 1 (Table 1). It does, however, provide a significantly improved geocellular rendering of cave morphology.

Models following Method 3 show an evident polynomial trend between the discretized volume and applied filter cut-off; with a coefficient of determination (R^2) of 1 (Fig. 13). This trend is consistent for the complete model as well as for the different segments, indicating that an optimal cut-off value can be determined if the "true" volume is known. Accurate volumetric modelling following Method 3 is then achievable by establishing an optimal geometric distance to the objects.

In this study, the applied point cloud density does not seem to have any impact on the modelling outcome in terms of volumetric rendering (Fig. 9D). Both point clouds (0.5m and 1.0m) result in models with identical volumes. However, the point densities used are below the applied global grid resolution, and thus a volumetric deviation might be expected as point density exceeds the grid resolution.

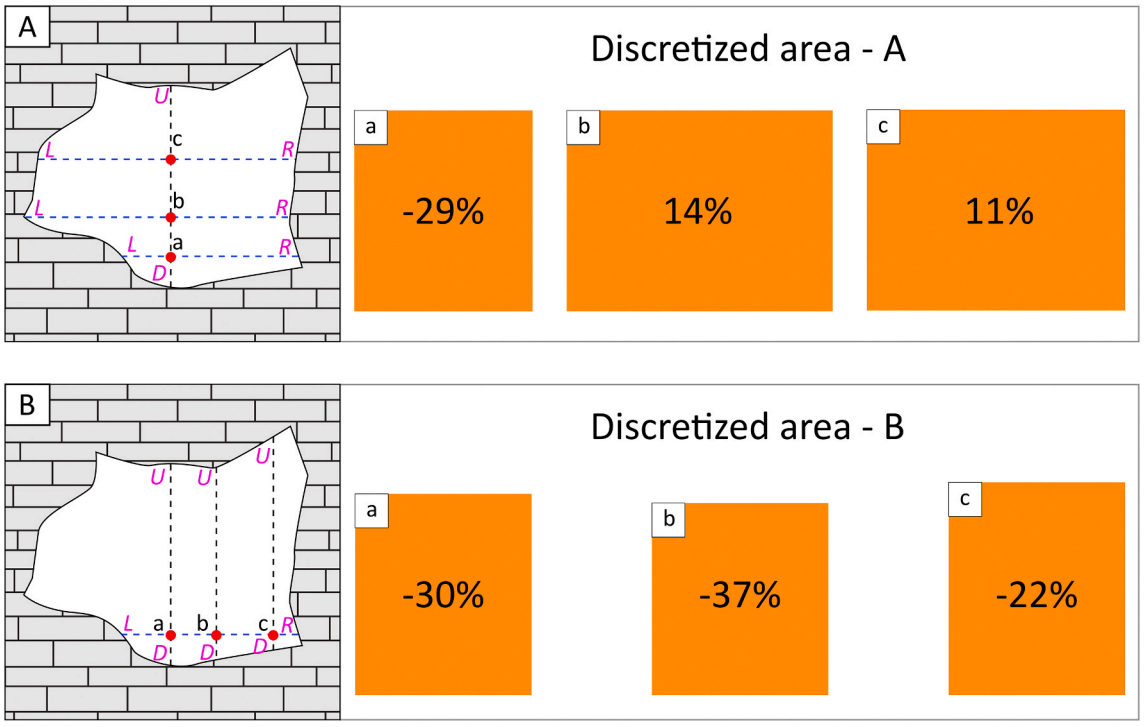

Fig. 18. Method 2 - Survey configuration and its impact on the cave representation in a geocellular framework. A) Example showing the horizontal impact of the vertical spatial distribution of the survey station. B) Example showing the vertical impact of the horizontal spatial distribution of the survey station. Right: The discretized areas (orange) and associated over-/underestimation, in percentage. Note that Method 2 renders all sections of the cave as rectangles causing significant deviation of the volumetric representation. (For interpretation of the references to colour in this figure legend, the reader is referred to the Web version of this article.)

Table 1
Methods summarized.

Method	Input data	Delineation	Rendered vol. (Mm^3)	Advantages	Disadvantages
Method 1	Center points	Geometric distance to centerline	1.13	Simple input data Time efficient	Cave geometry not captured Vol. accuracy dependant on morphological hetereogenity
Method 2	Center points + LRUD	Floor and roof horizons Wall polygon	2.66	Simple input data	Cave geometry not captured Time consuming Multi-tiered systems add complexity Overestimate vol.
Method 3	Centre points + multiple wall shots	Geometric distance to point cloud	1.55	Good geometric representation Good vol. representation	Geometric resolution reflects cave survey resolution Require "true" cave vol. to establish an optimal filter cut-off

The plot "cumulative length vs cumulative volume" (Fig. 10B) displays the continuous difference in area between the methods, which in turn reflects geometric heterogeneity. As observed in Fig. 9D, some of the Method 3 segments exhibit volumes that deviate from the "true" cave volume. However, the overall volume captured by Method 3 is close to that of the original cave survey (Fig. 10B).

5.4. Grid resolution and cut-off value

Grid resolution, as expected, influences geometric rendering and volumetric calculations in the models. The grid cell size sensitivity (Fig. 12) illustrates how rendered volume and cell-to-cell connectivity reflects the global grid resolution applied (e.g. Fig. 14). For Method 1 and 3, volumetric rendering is similar for any given cut-off value and global grid resolutions below 16 m^3. However, once the global grid resolution exceeds 8 m^3 the discretized volume decreases significantly. This could be explained by the grid cell size exceeding the conduit dimensions or that the distance to certain grid cell centre-points is surpassing the cut-off value.

Method 1 and 3 are very sensitive to the applied parameter cut-off value which must be equal to, or larger, than the grid cell resolution to ensure a coherent grid model of the cave system. On the other hand, for Method 2, grid cell connectivity is sensitive to the global grid cell resolution applied, and coherence diminishes in areas where the grid cell size exceeds the vertical and horizontal extent of the conduits (Fig. 12). Thus, all grid cells extruding the boundary surfaces and wall polygon will not be discretized.

In most cases, the use of very high-resolution grids (i.e. with cells $<2 \times 2 \times 2$m) is limited by CPU cost. However, as computer modelling and tracer tests have shown (e.g. Field and Pinsky, 2000; Hauns et al., 2001; Goldscheider, 2008; Montaron et al., 2014), morphology can substantially affect calculations of in-place volumes, fluid flow, and production behaviour and hence reserve estimates. Thus, ideally, modelling efforts should strive to incorporate as much geometric detail as possible without the model becoming unmanageable. On the other hand, the level of morphologic detail provided by using cave surveys is beyond anything achievable using seismic and well -data. In models of actual subsurface reservoirs, these morphological features must be captured using stochastic modelling methods. Constraints and guidelines for these can, however, be provided by using the kind of analogue models exemplified in the present study.

6. Conclusion

The method for implementing cave survey data into industry-standard reservoir models as presented here (Method 3), provides an significantly improved rendering compared to previous methods by Furnée (2015) and Ledsaak (2016).

The two pre-established methods systematically and significantly either overestimate or underestimate the actual cave volume. A volumetric over- or underestimation is expected when irregular shapes conform to a geocellular framework. This relates to the "edge-effect" caused by grid cell corners either extruding the cave periphery or when grid cells are not entirely infilling the cave volume. For Method 1 the accuracy of volumetric calculations is related to the accuracy of the estimated mean cave diameter employed as model input, whereas for Method 2 it is primarily related to all cave cross-sections being represented as rectangles.

As shown in this study, our proposed method (Method 3) provides a good approximation of the cave morphology and volume when employing cave surveys as input. The precision is limited by the quality of the survey, grid resolution and applied filter cut-off value. An optimal filter cut-off value can be determined if the "true" cave volume and desired global grid resolution is known, allowing geometric and volumetric accurate and coherent geocellular rendering.

A 3D geocellular model of the cave system in combination with conventional methods for gathering stratigraphic- and structural data, could be a good starting point for developing guidelines and workflows for forward collapse modelling. This combination would allow easy discretization of pre- and post-collapse infill and associated population of petrophysical properties. Moreover, using recent cave systems as analogues to paleokarst reservoir modelling may be appropriate as the tectonostratigraphic history of the cave systems is often well constrained and cave survey data ubiquitous.

CRediT authorship contribution statement

Bjarte Lønøy: Writing - original draft, Writing - review & editing, Conceptualization, Software, Data curation, Formal analysis, Investigation, Methodology, Validation, Visualization. **Jan Tveranger:** Writing - review & editing, Conceptualization, Formal analysis, Funding acquisition, Methodology, Project administration, Resources, Supervision, Validation. **Christos Pennos:** Writing - review & editing, Conceptualization, Methodology, Software, Resources, Validation. **Fiona Whitaker:** Writing - review & editing, Methodology, Supervision. **Stein-Erik Lauritzen:** Writing - review & editing, Supervision, Conceptualization.

Declaration of competing interest

The authors declare that they have no known competing financial interests or personal relationships that could have appeared to influence the work reported in this paper.

Acknowledgement

The authors would like to thank the Research Council of Norway (project number: 267634) for funding this study and Emerson Roxar for providing an academic license for RMS™. The reviewers are acknowledged for their constructive feedback and for improving the research. Jon Petter Furnee and Karina Ledsaak are acknowledged for their pioneering work in using cave survey data as input to paleokarst reservoir modelling. The scientific discussions with Gordon Coy, Mateu Esteban Cerdà and Arve Lønøy (the latter also contributed by proof-reading) are also highly appreciated, and their input has significantly benefited the research.

Appendix A. Supplementary data

Supplementary data to this article can be found online at https://doi.org/10.1016/j.marpetgeo.2020.104652.

References

Blickwede, J., Rosenfeld, J., 2010. The Greatest Oil Well in History? the Story of Cerro Azul# 4.
Borghi, A., Renard, P., Jenni, S., 2010. How to model realistic 3D karst reservoirs using a pseudo-genetic methodology–example of two case studies. Advances in Research in Karst Media 251–255.
Branets, L.V., Ghai, S.S., Lyons, S.L., Wu, X.H., 2009. Challenges and technologies in reservoir modeling. Commun. Comput. Phys. 6, 1–23.
Budaj, M., Mudrák, S., 2008. Therion–digital cave maps therion–cartographie souterraine digitale. In: Presented on the 4th European Speleological Congress. Banska Bystrica, Slovakia.
Budaj, M., Stacho, M., 2019. Therion 5.4, 4 ed.
Chaojun, Z., Chengzao, J., Benliang, L., Xiuyu, L., Yunxiang, L., 2010. Ancient karsts and hydrocarbon accumulation in the middle and western parts of the North Tarim uplift, NW China. Petrol. Explor. Dev. 37, 263–269.
Coogan, A.H., Maggio, C., Bebout, D.G., 1972. Depositional environments and geologic history of golden Lane and poza rica trend, Mexico, an alternative view. Am. Assoc. Petrol. Geol. Bull. 56, 1419–&.
Craig, D.H., 1988. Caves and Other Features of Permian Karst in San Andres Dolomite, Yates Field Reservoir. Springer, west Texas, Paleokarst, pp. 342–363.
Curl, R.L., 1986. Fractal dimensions and geometries of caves. Math. Geol. 18, 765–783.
Erzeybek Balan, S., 2012. Characterization and Modeling of Paleokarst Reservoirs Using Multiple-point Statistics on a Non-gridded Basis. The University of Texas at Austin, pp. 1–307. Ph.D. Dissertation.
Field, M.S., Pinsky, P.F., 2000. A two-region nonequilibrium model for solute transport in solution conduits in karstic aquifers. J. Contam. Hydrol. 44, 329–351.
Fikos, I., Vargemezis, G., Pennos, C., Lønøy, B., Jensen, K., Tveranger, J., EAGE, 2019. Processing 2D ERT data in 3D environment: a case study inside a karstic cave in North Greece. In: Near Surface Geoscience Conference and Exhibition. The Hauge, Netherlands.
Fournillon, A., Abelard, S., Viseur, S., Arfib, B., Borgomano, J., 2012. Characterization of karstic networks by automatic extraction of geometrical and topological parameters: comparison between observations and stochastic simulations. Geological Society, London, Special Publications 370, 247–264.
Furnée, J.P.B., 2015. Geo-modeling and Fluid Flow Simulation in Paleokarst Reservoirs. The University of Bergen.
Gallay, M., Hochmuth, Z., Kanuk, J., Hofierka, J., 2016. Geomorphometric analysis of cave ceiling channels mapped with 3-D terrestrial laser scanning. Hydrol. Earth Syst. Sci. 20, 1827–1849.
Gallay, M., Kanuk, J., Hochmuth, Z., Meneely, J.D., Hofierka, J., Sedlak, V., 2015. Large-scale and high-resolution 3-D cave mapping by terrestrial laser scanning: a case study of the Domica Cave, Slovakia. Int. J. Speleol. 44, 277–291.
Gede, M., Petters, C., Nagy, G., Nagy, A., Mészáros, J., Kovács, B., Egri, C., 2013. Laser scanning survey in the pálvölgy cave, budapest. In: Proceedings of the 26th International Cartographic Conference. International Cartographic Association, Dresden, p. 905.
Goldscheider, N., 2008. A new quantitative interpretation of the long-tail and plateau-like breakthrough curves from tracer tests in the artesian karst aquifer of Stuttgart, Germany. Hydrogeol. J. 16, 1311–1317.
Hauns, M., Jeannin, P.Y., Atteia, O., 2001. Dispersion, retardation and scale effect in tracer breakthrough curves in karst conduits. J. Hydrol. 241, 177–193.
Heeb, B., 2008. Paperless Caving-An Electronic Cave Surveying System La topo sans papier-un système électronique de topographie. IV th European speleological congress (Isére - France).
Heeb, B., 2009. An all-in-one electronic cave surveying device. Cave Radio & Electronics Group Journal 72, 8–10.
Heeb, B., 2010. PocketTopo 1.34.
Heeb, B., 2014. The next generation of the DistoX cave surveying instrument. CREG Journal 88, 5–8.
Kaiser, M.J., Pulsipher, A.G., 2007. A review of the oil and gas sector in Kazakhstan. Energy Pol. 35, 1300–1314.
Labourdette, R., Lascu, I., Mylroie, J., Roth, M., 2007. Process-like modeling of flank-margin caves: from genesis to burial evolution. J. Sediment. Res. 77, 965–979.
Ledsaak, K., 2016. Geo-modelling of Paleokarst Reservoirs-From Cave-Survey to Geocellular Paleokarst Model. The University of Bergen.
Lerma, J.L., Navarro, S., Cabrelles, M., Villaverde, V., 2010. Terrestrial laser scanning and close range photogrammetry for 3D archaeological documentation: the Upper Palaeolithic Cave of Parpallo as a case study. J. Archaeol. Sci. 37, 499–507.
Lomando, A.J., Harris, P.M., Orlopp, D.E., 1993. Casablanca Field, Tarragona Basin, Offshore Spain: a Karsted Carbonate Reservoir. Special publications of SEPM.
Lønøy, B., Pennos, C., Tveranger, J., Fikos, I., Vargemezis, G., Jensen, K., Lauritzen, S.-E., 2019a. Sediment Accumulations in Paleokarst Reservoirs - Analogues from an Active Cave System. Bathurst Meeting of Carbonate Sedimentologists 2019, Mallorca, Spain, p. 1.
Lønøy, B., Pennos, C., Tveranger, J., Lauritzen, S.-E., Furnée, J.P., Ledsaak, K., 2019b. Paleokarst Reservoir Modelling Based on Active Cave System Analogs - Implementing Cave Survey Data in Geocellular Reservoir Models. Winter conference 2019. Bergen.

Loucks, R.G., 1999. Paleocave carbonate reservoirs: origins, burial-depth modifications, spatial complexity, and reservoir implications. AAPG Bull. 83, 1795–1834.
Lu, X.B., Wang, Y., Tian, F., Li, X.H., Yang, D.B., Li, T., Lv, Y.P., He, X.M., 2017. New insights into the carbonate karstic fault system and reservoir formation in the Southern Tahe area of the Tarim Basin. Mar. Petrol. Geol. 86, 587–605.
Mallison, B., Sword, C., Viard, T., Milliken, W., Cheng, A., 2014. Unstructured cut-cell grids for modeling complex reservoirs. SPE J. 19, 340–352.
MATLAB, 2010. Version 9.4.0.813654. The MathWorks Inc, Natick, Massachusetts. R2018a.
Montaron, B., 2008. Carbonate evolution. Oil & Gas Middle East, pp. 26–31.
Montaron, B.A., Xue, F.J., Tian, W., Han, R., Ray, P., 2014. Cave Geomorphology and its Effects on Oil Recovery Factors in Tarim Karst Reservoirs, West China, International Petroleum Technology Conference. Kuala Lumpur, Malaysia, p. 13.
Mylroie, J.E., Carew, J.L., 1995. Karst Development on Carbonate Islands.
Palmer, A.N., 1991. Origin and morphology of limestone caves. Geol. Soc. Am. Bull. 103, 1–21.
Pardo-Igúzquiza, E., Dowd, P.A., Durán, J.J., Robledo-Ardila, P., 2018. A review of fractals in karst. Int. J. Speleol. 48, 2.
Pennos, C., Lauritzen, S.E., Pechlivanidou, S., Aidona, E., Haflidason, H., Sotiriadis, Y., 2016a. Decoding Clastic Sediment Sources from the Maaras Cave Northern Greece, 18th Joint Geomorphological Meeting. Chambery, France.
Pennos, C., Lauritzen, S.E., Pechlivanidou, S., Sotiriadis, Y., 2016b. Geomorphic constrains on the evolution of the Aggitis river basin Northern Greece. Bull. Geol. Soc. Greece 50.
Rongier, G., Collon-Drouaillet, P., Filipponi, M., 2014. Simulation of 3D karst conduits with an object-distance based method integrating geological knowledge. Geomorphology 217, 152–164.
Roxar, R.M.S., 2018. Roxar Software Solutions 1994-2018, 11.0.1 ed.
Soudet, H.J., Sorriaux, P., Rolando, J.P., 1994. Relationship between fractures and karstification - the oil-bearing paleokarst of Rospo Mare (Italy). B Cent Rech Expl 18, 257–297.
Sun, S.Q., Sloan, R., 2003. Quantification of uncertainty in recovery efficiency predictions: lessons learned from 250 mature carbonate fields. In: SPE Annual Technical Conference and Exhibition. Society of Petroleum Engineers, Denver, Colorado, p. 15.
Tian, F., Jin, Q., Lu, X.B., Lei, Y.H., Zhang, L.K., Zheng, S.Q., Zhang, H.F., Rong, Y.S., Liu, N.G., 2016. Multi-layered ordovician paleokarst reservoir detection and spatial delineation: a case study in the Tahe Oilfield, Tarim Basin, Western China. Mar. Petrol. Geol. 69, 53–73.
Trice, R., 2005. Challenges and insights in optimising oil production form middle eastern karst reservoirs. In: SPE Middle East Oil and Gas Show and Conference. Society of Petroleum Engineers.
Viniegra, F., Castillo-Tejero, C., 1970. Golden Lane Fields. Veracruz, Mexico.
Visual Topo, 2017. David, Eric, 5.06.
Weisstein, E.W., 2020. Polygon area, from MathWorld–A wolfram web resource. http://mathworld.wolfram.com/PolygonArea.html.
White, W.B., Culver, D.C., Herman, J.S., Kane, T.C., Mylroie, J.E., 1995. Karst lands. Am. Sci. 83, 450–459.
Yan, X., 2002. Reservoir properties of ordovician carbonate rocks in the Tahe field, Tarim Basin, China. Shiyou Yu Tianranqi Dizh (Oil and Gas Geology) 23, 262–265.
Zempolich, W.G., Cook, H.E., 2002. Paleozoic carbonates of the Commonwealth of Independent States (CIS): subsurface reservoirs and outcrop analogues, Paleozoic carbonates of the Commonwealth of Independent States (CIS): subsurface reservoirs and outcrop analogues. SEPM Society for Sedimentary Geology, Special publications of SEPM, pp. 1–3.